CC BY

http://dx.doi.org/10.35596/1729-7648-2026-24-5-51-59

UDC 621.396.96

ESTIMATION OF THE ANGULAR TURN RATE OF AN AIRBORNE OBJECT BASED ON THE UNSCENTED TRANSFORMATION OF AN AUGMENTED STATE VECTOR

PETR KHMARSKI[1], VALENTIN ARTEMIEV[1], ALEXANDER NAUMOV[1], ALEXANDER BONDARENKO[2], BOBOMUROD MUXAMMEDOV[3]

[1]Institute of Applied Physics of the National Academy of Sciences of Belarus (Minsk, Republic of Belarus)
[2]Military Academy of the Republic of Belarus (Minsk, Republic of Belarus)
[3]Institute of Military Aviation of the University of Military Security and Defense of the Republic of Uzbekistan (Qarshi, Republic of Uzbekistan)

Abstract. A discrete filter is examined for the joint estimation of the coordinates, velocity, and angular rate Ω of a target performing a steady turn, based on indirect (polar/spherical) radar measurements. When Ω is included in the augmented state vector, the increment conversion matrix becomes a nonlinear function of Ω itself; consequently, linearization – as employed in previously studied versions of the extended Kalman filter for indirect measurements – requires recalculating the Jacobian matrix at each step and introduces an additional methodological error. An unscented transformation of the augmented state vector is proposed to eliminate the need for linearizing the motion and measurement models. Monte Carlo statistical simulations (N_{run} = 545) were conducted to compare the proposed algorithm with its linearized counterpart across eight standard surveillance radar types (2D and 3D) and five target turn rates. The results demonstrate that the proposed algorithm yields a root-mean-square error for the Ω estimate that is, on average, 4.3 times lower (median 4.0; range 1.4–14.0 across all observation conditions) than that of the linearized extended Kalman filter, while offering a more modest improvement (averaging 1.2 times) in the root-mean-square error of the position estimate.

Keywords: extended Kalman filter, unscented transform, steady-state turn, target angular rate, maneuvering target, linearization, Jacobian matrix, Monte Carlo method, radar station.

Conflict of interests. The authors declare that there is no conflict of interests.

For citation. Khmarski P., Artemiev V., Naumov A., Bondarenko A., Muxammedov B. (2026) Estimation of the Angular Turn Rate of an Airborne Object Based on the Unscented Transformation of an Augmented State Vector. *Doklady BGUIR*. 24 (5), 51–59. http://dx.doi.org/10.35596/1729-7648-2026-24-5-51-59.

ОЦЕНИВАНИЕ УГЛОВОЙ СКОРОСТИ РАЗВОРОТА ВОЗДУШНОГО ОБЪЕКТА НА ОСНОВЕ АНСЦЕНТНОГО ПРЕОБРАЗОВАНИЯ РАСШИРЕННОГО ВЕКТОРА СОСТОЯНИЯ

П. А. ХМАРСКИЙ[1], В. М. АРТЕМЬЕВ[1], А. О. НАУМОВ[1], А. Е. БОНДАРЕНКО[2], Б. М. МУХАММЕДОВ[3]

[1]Институт прикладной физики Национальной академии наук Беларуси (Минск, Республика Беларусь)
[2]Военная академия Республики Беларусь (Минск, Республика Беларусь)
[3]Институт военной авиации Университета военной безопасности и обороны Республики Узбекистан (Карши, Республика Узбекистан)

Аннотация. Рассмотрен дискретный фильтр совместного оценивания координат, скорости и угловой скорости Ω цели, совершающей установившийся разворот, по косвенным (полярным/сферическим) измерениям радиолокационных станций. При включении Ω в расширенный вектор состояния матрица пересчета приращений становится нелинейной функцией самой Ω, поэтому линеаризация (используемая в ранее рассмотренных модификациях расширенного фильтра Кальмана при косвенных измерениях) требует пересчета матрицы Якоби на каждом шаге и вносит дополнительную методическую ошибку. Предложено ансцентное преобразование расширенного вектора состояния, исключающее линеаризацию модели движе-

ния и измерения. Проведено статистическое моделирование методом Монте-Карло ($N_{оп}$ = 545) алгоритма и его линеаризованного аналога для восьми типовых радиолокационных станций кругового обзора (2D и 3D) и пяти значений угловой скорости разворота цели. Показано, что предложенный алгоритм обеспечивает среднеквадратическое отклонение оценки Ω в среднем в 4,3 раза (медиана 4,0, разброс 1,4–14,0 по всей матрице условий наблюдения) меньше, чем расширенный фильтр Кальмана при косвенных измерениях с линеаризацией, при заметно более скромном (в среднем 1,2 раза) выигрыше по среднеквадратическому отклонению местоположения.

Ключевые слова: расширенный фильтр Калмана, ансцентное преобразование, установившийся разворот, угловая скорость цели, маневрирующая цель, линеаризация, матрица Якоби, метод Монте-Карло, радиолокационная станция.

Конфликт интересов. Авторы заявляют об отсутствии конфликта интересов.

Для цитирования. Оценивание угловой скорости разворота воздушного объекта на основе ансцентного преобразования расширенного вектора состояния / П. А. Хмарский [и др.] // Доклады БГУИР. 2026. Т. 24, № 5. С. 51–59. http://dx.doi.org/10.35596/1729-7648-2026-24-5-51-59.

Introduction

Measuring aircraft coordinates and motion parameters from primary (indirect) observations – single-scan estimates of range r, azimuth β and, for three-coordinate radars, elevation angle ε – is a principal task of radar surveillance [1]; propagation-related errors are addressed separately, e. g. in [2]. Kalman filter (KF) synthesis rests on a motion (driving-input) model; for a maneuvering target, the constant-velocity model ceases to match the actual trajectory, increasing the filtering error and, in the limit, causing track loss [3]. A common approach to describing a horizontal maneuver is the coordinated-turn (CT) model [4], with constant speed and constant turn rate Ω; KF design for indirect measurements under this model is examined in [5]. In this work, as in most known sources [3, 4], Ω-filtering augments the state vector with Ω and linearizes both the nonlinear motion and measurement models.

Recent work on nonlinear filtering for maneuvering targets includes: unscented/cubature KF modifications, for targets in general [6–8] and turning targets under angle-only measurements [9]; robust/adaptive extended Kalman filter (EKF) modifications compensating for linearization error [10–12], confirmed by Monte-Carlo methods [13]; alternative parameterizations linearizing only the measurement model [14, 15]; adaptive multiple-hypothesis schemes [16]; and direct turn-rate estimation outside the motion model [17]. None, however, addresses estimating Ω once included in the CT model's augmented state vector – the question examined here.

Work [18] demonstrates by Monte-Carlo methods, that how well linearization approximates the Gaussian density depends substantially on observation conditions (σβ, range r, heading angle) and can cause errors up to track loss. Because including Ω makes the state-transition matrix $\mathbf{B}$ itself nonlinear in Ω (see $\mathbf{B}_k$ [5]), linearization errors are expected not only in the measurement Jacobian, as in [18], but also during prediction – critically for Ω, a parameter for which [5, 18] give no accuracy figures. The goal of this paper is a comparative analysis of the accuracy with which the turn rate Ω, position, and speed of a target performing a coordinated turn and observed through indirect radar measurements are estimated, using a discrete filter based on the unscented transform and its linearized (extended) counterpart.

Problem statement

Initial conditions. Let the observed parameter vector $\boldsymbol{\theta}$ comprise single-scan estimates of slant range r, azimuth β and, for a three-coordinate radar, elevation angle ε:

$$\boldsymbol{\theta} = \begin{cases} \|r \quad \beta\|^{\mathrm{T}}, \ \text{2D radar;} \\ \|r \quad \beta \quad \varepsilon\|^{\mathrm{T}}, \ \text{3D radar.} \end{cases} \tag{1}$$

Observation errors are uncorrelated and characterized by the covariance matrix $\mathbf{R}_\theta = \mathrm{diag}(\sigma_r^2, \sigma_\beta^2, \sigma_\varepsilon^2)$, where $\sigma_r, \sigma_\beta, \sigma_\varepsilon$ are the range, azimuth and elevation observation-error standard deviations. The scan period equals T.

The target is an aircraft performing a coordinated turn in the horizontal plane at constant speed v and constant turn rate Ω. The estimated state vector

$$\boldsymbol{\alpha} = \left\| x \quad \dot{x} \quad z \quad \dot{z} \quad y \quad \dot{y} \quad \Omega \right\|^{\mathrm{T}} \tag{2}$$

includes single-scan estimates of the Cartesian coordinates x (north), z (east), y (altitude), their rates of change, and the turn rate Ω, following [5] but with an added altitude channel for three-coordinate radars; a two-coordinate radar carries no elevation information, so this channel is not corrected by the filter (see below).

Objectives:

1) examine the features of a discrete KF design that uses the unscented transform to jointly estimate **α**, Ω included, without linearizing either the motion or measurement model;

2) use Monte-Carlo modeling to compare the Ω, position, and speed accuracy of the proposed algorithm against the linearized extended KF for indirect measurements, for eight representative circular-scan radars and five values of Ω.

Features of filter design for estimating coordinated-turn parameters

Motion and measurement models. The CT dynamic model for the Cartesian coordinates and velocities $\left\| x \quad \dot{x} \quad z \quad \dot{z} \right\|^{\mathrm{T}}$ is nonlinear in Ω and at step k is written as [5]:

$$x_{k+1} = x_k + \frac{\sin(\Omega_k T)}{\Omega_k}\dot{x}_k - \frac{1-\cos(\Omega_k T)}{\Omega_k}\dot{z}_k;\ \ \dot{x}_{k+1} = \cos(\Omega_k T)\dot{x}_k - \sin(\Omega_k T)\dot{z}_k;$$

$$z_{k+1} = z_k + \frac{1-\cos(\Omega_k T)}{\Omega_k}\dot{x}_k + \frac{\sin(\Omega_k T)}{\Omega_k}\dot{z}_k;\ \ \dot{z}_{k+1} = \sin(\Omega_k T)\dot{x}_k + \cos(\Omega_k T)\dot{z}_k;$$

$$y_{k+1} = y_k + \dot{y}_k T;\ \ \dot{y}_{k+1} = \dot{y}_k. \tag{3}$$

This represents, compact form is a nonlinear state-transition vector function $\boldsymbol{\alpha}_{k+1} = \mathbf{b}(\boldsymbol{\alpha}_k) + \xi_{k+1}$, where ξ_{k+1} is the random discrete-maneuver (process) noise (see below); once Ω is included in (2), the turn rate is treated as slowly varying, with a random increment: $\Omega_{k+1} = \Omega_k + \eta_{k+1}$, $\eta_{k+1} \sim N(0, \sigma_\Omega^2 T)$.

The measurement model for a three-coordinate radar is (analogous to [19])

$$\mathbf{h}(\boldsymbol{\alpha}) = \left\| \begin{matrix} \sqrt{x^2 + z^2 + y^2} \\ \operatorname{arctg}(x / z) \\ \arcsin(y / \sqrt{x^2 + z^2 + y^2}) \end{matrix} \right\|. \tag{4}$$

For a two-coordinate radar, the first two rows of (4) without the elevation channel.

State-transition matrix: dependence on the turn rate. The key feature of filtering coordinated-turn parameters is that Ω not only governs how the coordinates and velocities evolve (3), but is itself a component of the differentiated state vector (2), so the deterministic state-transition matrix **B** [20]

$$\mathbf{B}_k = \partial \mathbf{b}(\boldsymbol{\alpha}) / \partial \boldsymbol{\alpha} \big|_{\boldsymbol{\alpha} = \hat{\boldsymbol{\alpha}}_k}. \tag{5}$$

Formula (5) contains, beyond the trigonometric rotation coefficients depending on Ω_k (as in the classical CT model with known Ω), an added column of partial derivatives $\partial\mathbf{b}/\partial\Omega$, since Ω is itself differentiated. Restricting to the block $\left\| x \quad \dot{x} \quad z \quad \dot{z} \quad \Omega \right\|^{\mathrm{T}}$ (the altitude channel $\left\| y \quad \dot{y} \right\|^{\mathrm{T}}$ does not depend on Ω and is recomputed trivially: $y_{k+1} = y_k + \dot{y}_k T$), matrix (5) takes the form [5]:

$$\mathbf{B}_k = \left\| \begin{matrix} 1 & \frac{\sin\Omega_k T}{\Omega_k} & 0 & -\frac{1-\cos\Omega_k T}{\Omega_k} & b_{15} \\ 0 & \cos\Omega_k T & 0 & -\sin\Omega_k T & -T\left(\dot{x}_k \sin\Omega_k T + \dot{z}_k \cos\Omega_k T\right) \\ 0 & \frac{1-\cos\Omega_k T}{\Omega_k} & 1 & \frac{\sin\Omega_k T}{\Omega_k} & b_{35} \\ 0 & \sin\Omega_k T & 0 & \cos\Omega_k T & T\left(\dot{x}_k \cos\Omega_k T - \dot{z}_k \sin\Omega_k T\right) \\ 0 & 0 & 0 & 0 & 1 \end{matrix} \right\|; \tag{6}$$

$$b_{15} = \left(T\Omega_k\left(\dot{x}_k\cos\Omega_k T - \dot{z}_k\sin\Omega_k T\right) - \dot{x}_k\sin\Omega_k T - \dot{z}_k\left(\cos\Omega_k T - 1\right)\right)\Big/\Omega_k^2;$$
$$b_{35} = \left(T\Omega_k\left(\dot{x}_k\sin\Omega_k T + \dot{z}_k\cos\Omega_k T\right) - \dot{x}_k\left(1 - \cos\Omega_k T\right) - \dot{z}_k\sin\Omega_k T\right)\Big/\Omega_k^2. \quad (7)$$

The elements b_{15}, b_{35} (the partial derivatives $\partial x_{k+1}/\partial\Omega_k$ and $\partial z_{k+1}/\partial\Omega_k$) contain Ω_k squared in the denominator, with no well-defined limit under linearization; they are recomputed every step from the current Ω_k, unlike the first four columns of (6), linear in $\left\|x \quad \dot{x} \quad z \quad \dot{z}\right\|^{\mathrm{T}}$ for fixed Ω; the last row of (6) reflects the model $\Omega_{k+1} = \Omega_k + \eta_k$ (Ω is not recomputed from the coordinates and velocities).

Unobservability of the turn rate in the measurement Jacobian. The measurement Jacobian $\mathbf{H}_k = \partial\mathbf{h}(\boldsymbol{\alpha})/\partial\boldsymbol{\alpha}\big|_{\boldsymbol{\alpha}=\hat{\boldsymbol{\alpha}}_{0k}}$ for measurement model (4) is (for a 3D radar, $r = \sqrt{x^2+z^2+y^2}$, $\rho = \sqrt{x^2+z^2}$):

$$\mathbf{H}_k = \begin{Vmatrix} x/r & 0 & z/r & 0 & y/r & 0 & 0 \\ z/\rho^2 & 0 & -x/\rho^2 & 0 & 0 & 0 & 0 \\ -xy/(r^2\rho) & 0 & -zy/(r^2\rho) & 0 & \rho/r^2 & 0 & 0 \end{Vmatrix}. \quad (8)$$

The essential feature of (8) is that the entire Ω column (like the velocity columns x, z, y) is identically zero: range, azimuth and elevation do not depend explicitly on velocity or turn rate, so Ω is unobservable from a single measurement $\boldsymbol{\theta}_{k+1}$, unlike the coordinates, for which $\mathbf{H}_k$ has nonzero elements. This holds exactly for both the linearized and exact measurement function, so the linearization error for Ω arises not at the update step but during prediction, through $\mathbf{B}_k$ (6) – unlike the general conclusion of [18] on measurement-model linearization errors.

Turn-rate estimation through cross-covariance. Since $\mathbf{H}_k[:,\Omega] \equiv \mathbf{0}$, correcting Ω from the measurement residual is possible only through a nonzero Ω-coordinate cross-covariance in the predicted-error covariance matrix. For the linearized EKF, the row of the gain matrix $\mathbf{K}_{k+1}$ corresponding to Ω equals

$$\mathbf{K}_{k+1}[\Omega,:] = \mathbf{R}_{0(k+1)}[\Omega,:]\mathbf{H}_k^T\left(\mathbf{H}_k\mathbf{R}_{0(k+1)}\mathbf{H}_k^{\mathrm{T}} + \mathbf{R}_\theta\right)^{-1}. \quad (9)$$

It is identically zero if the elements $\mathbf{R}_{0(k+1)}[\Omega, x]$, $\mathbf{R}_{0(k+1)}[\Omega, z]$ (Ω's cross-covariance with the coordinates) are zero; by (6), (7), the prediction step $\mathbf{R}_{0(k+1)} = \mathbf{B}_k\mathbf{R}_k\mathbf{B}_k^T + \mathbf{M}_k$ generates it (through the nonzero elements b_{15}, b_{35}, and also through $\mathbf{R}_k[\Omega,\Omega]$, nonzero from the outset owing to the a priori uncertainty in Ω_0) – that is, the turn rate is estimated not from the measurement itself, but from how its uncertainty at the previous step "colors" the predicted position uncertainty at the current step. This is why Ω converges only after several steps, unlike the coordinates, corrected at the first.

Setting the filter's initial values by weighted least squares. Because correcting Ω proceeds only through the cross-covariance (see above), the initial estimate's quality substantially affects convergence speed. No a priori information about the target (speed, heading) is available – only the plots, the radar's rated accuracies, and the scan period – so the entire state vector, Ω included, is estimated from the first K_0 plots by weighted least squares (WLS), referred to below simply as initialization (not to be confused with track initiation: plot-to-target assignment is assumed given, and the problem reduces to estimating the initial state of an already-known object).

Each plot is converted to Cartesian coordinates, its covariance through the Jacobian of that conversion, $\mathbf{R}_{xyz} = \mathbf{J}\mathbf{R}_0\mathbf{J}^{\mathrm{T}}$; their inverses form the weight matrix $\mathbf{W}$. The position at plot j is a deterministic function of the state vector, $\mathbf{p}_j = \mathbf{H}_p\mathbf{F}(\Omega, t_j)\mathbf{s}$, where $\mathbf{s}$ is its linear part, $\mathbf{H}_p$ selects the coordinates and $t_j = (j - K_0 + 1)T$. The last plot is taken as the reference instant, and filtering starts from it.

The essential point is that for a fixed Ω the model is linear in $\mathbf{s}$. The problem is thus separable: the linear part is obtained in closed form, and the search runs over a single parameter

$$\hat{\mathbf{s}}(\Omega) = \left(\mathbf{A}^{\mathrm{T}}\mathbf{W}\mathbf{A}\right)^{-1}\mathbf{A}^{\mathrm{T}}\mathbf{W}\tilde{\mathbf{p}};\ \ \hat{\Omega} = \arg\min_{\Omega}\boldsymbol{\nu}^{\mathrm{T}}(\Omega)\mathbf{W}\boldsymbol{\nu}(\Omega);\ \ \boldsymbol{\nu}(\Omega) = \tilde{\mathbf{p}} - \mathbf{A}(\Omega)\hat{\mathbf{s}}(\Omega), \quad (10)$$

where the rows of $\mathbf{A}(\Omega)$ are $\mathbf{H}_p\mathbf{F}(\Omega, t_j)$ and $\tilde{\mathbf{p}}$ is the vector of converted plots. No initial guess is needed for the linear part, unlike iterative minimization over the whole vector.

For $K_0 = 2$ the system is underdetermined (six equations for seven unknowns for a three-coordinate radar, four for five for a two-coordinate one), so $K_0 \geq 3$, increased until the Ω estimate's standard deviation becomes acceptable. The search over Ω is confined to $|\Omega| < 180°/T$, beyond which Ω and $\Omega \pm 360°/T$ are indistinguishable.

The covariance of the initial errors is taken from the estimation procedure itself: Gauss–Newton linearization underestimates the spread in Ω (entering only through the trajectory's curvature, with a flat minimum for large noise), so it is obtained instead by a parametric bootstrap: "ideal" plots are reconstructed from the estimate, perturbed with the known $\mathbf{R}_0$, and passed through the whole estimator again:

$$\mathbf{R}_0 = \frac{1}{M-1}\sum_{i=1}^{M}\left(\hat{\boldsymbol{\alpha}}^{(i)} - \bar{\boldsymbol{\alpha}}\right)\left(\hat{\boldsymbol{\alpha}}^{(i)} - \bar{\boldsymbol{\alpha}}\right)^{\mathrm{T}} + \left(\mathbf{G}^{\mathrm{T}}\mathbf{W}\mathbf{G}\right)^{-1}, \tag{11}$$

where $\hat{\boldsymbol{\alpha}}^{(i)}$ are the estimates over M ensemble realizations; $\bar{\boldsymbol{\alpha}}$ is their mean; $G = \left[\mathbf{A} \middle| \left(\partial\mathbf{A}/\partial\Omega\right)\hat{\mathbf{s}}\right]$ is the augmented Jacobian.

The second term regularizes, since the sample covariance over a finite ensemble is near-singular and inverting it would produce outliers.

A limitation of the linearized extended Kalman filter. The elements b_{15}, b_{35} of matrix (6) are recomputed at every step from the current estimate Ω_k, and, by [18], their linearization error grows with increasing $\Omega_k T$ – precisely for an intense maneuver or a sparse scan (large T). This is the motivation for switching to the unscented transform, which needs neither $\mathbf{B}_k$ nor $\mathbf{H}_k$ computed explicitly.

Unscented transform of the augmented state vector. The unscented transform approximates the posterior density not by linearizing, but by propagating a deterministic set of sigma points whose mean and covariance match the approximated Gaussian [21]. For indirect (polar) measurements, sigma-point generation and the prediction–update recursions are given in full in [22] and not repeated here; specific to state vector (2) is only that the process-noise covariance is augmented with the turn-rate increment's variance on the Ω diagonal entry, giving $n = 7$ ($2n + 1 = 15$ sigma points). No Jacobian $\mathbf{B}_k$ or $\mathbf{H}_k$ is computed: the exact transforms (3), (4) apply directly to each sigma point, approximating mean and covariance to at least second-order accuracy for any nonlinearity, versus first-order for linearization [21].

The cross-covariance mechanism described above still operates here without an explicit $\mathbf{H}_k$: sigma points differing only in Ω yield different predicted coordinates during prediction (3), and only these differing coordinates, once propagated through $\mathbf{h}(\cdot)$, produce a nonzero cross-covariance in measurement space. The sensitivity of the measurement to Ω is thus formed entirely through the prediction step – qualitatively similar to the linearized algorithm's mechanism, but quantitatively different in how accurately that sensitivity transfers for large ΩT (see below).

Results of statistical modeling

A comparative simulation of the proposed unscented KF (UKF) and its linearized extended-KF counterpart (EKF; equivalent to Filter 3 of [5]) covered eight representative circular-scan radars (Tab. 1: four two- and four three-coordinate) and five turn rates $\Omega \in \{3, 6, 8, 10, 15\}$°/s at speed v = 250 m/s, onset range $r_0 = R_{\max}/2$, 70 s maneuver duration – 40 radar×Ω combinations. The quality measure was the parameter root-mean-square error (RMSE), ΔΩ, Δpos, computed as for $\Delta\Sigma(k)$ in [19] (averaged over N_{run} = 545 realizations); for two-coordinate radars, Δpos used only the horizontal coordinates x, z, excluding the altitude channel y – unobservable here (a zero column in (8)) and, unlike Ω, not coupled to Ω, x, z through $\mathbf{B}_k$ (see above), so its error reflects only the arbitrary initial guess, not filter quality.

Table 1. Main characteristics of the representative circular-scan surveillance radars used in the modeling

Radar	Application	Band	Type	$R_{\max}$, km	T, s	σ_r, m	σ_β, deg.	σ_ε, deg.
R1	Small-UAV monitoring	X	2D	15	9	7.5	0.50°	–
R2	Aerodrome surveillance (ATC)	L	2D	110	6	100	0.40°	–
R3	Long-range air surveillance	VHF	2D	360	5	25	0.83°	–
R4	En-route surveillance (ATC)	VHF	2D	360	10	25	0.50°	–
R5	Aerodrome airspace monitoring	X	3D	25	2	30	0.30°	0.50°
R6	Precision approach	X	3D	40	1	20	0.30°	0.30°
R7	Long-range 3D surveillance	S	3D	470	4	100	0.20°	0.50°
R8	3D en-route surveillance	VHF/S	3D	360	10	25	0.80°	0.10°

For position and speed RMSE, a potentially achievable error is additionally reported: the result from the same unscented filter when Ω is known exactly and supplied as a fixed motion-model parameter (state dimension n = 6), with the measurement nonlinearity still handled by the unscented transform.

Not physically realizable (the true Ω is unknown in advance), this filter serves as a lower bound showing how much of the error is due to measurement noise alone versus not knowing Ω; the comparison is graphical only, with no bound drawn for turn-rate RMSE, whose error is identically zero when Ω is known.

All three algorithms start from the same initialization, computed once per realization, so the comparison is not confounded with initialization quality; the known-Ω benchmark uses the same number of initialization plots as the others (though a shorter one would suffice), keeping the curves comparable step by step. The RMSE is averaged from $k \geq K_0 - 1$ onward, i. e. from the initialization window's reference plot, since no estimates exist before it.

The results (Tab. 2) show that, at Ω = 6°/s, the UKF's Ω RMSE (0.8–1.0 deg./s) is 2.3× (R4) to 10,0× (R3) smaller than the EKF's (2.0–9.3 deg./s). Across the 40 radarЧΩ combinations, the UKF's gain averages 4.3× in ΔΩ (median 4.0; range 1.4–14.0) and 3.8× in ΔV (median 2.8; range 0.99–19.7), but only 1.2× in Δpos (range 1.0–1.9) – confirming the mechanism above: coordinates are corrected directly (nonzero $\mathbf{H}_k$), while Ω and speed (also a zero $\mathbf{H}_k$ column) are corrected only through the cross-covariance from $\mathbf{B}_k$. The ΔV gain ranges from near unity (Ω = 3°/s) to nearly 20× for R3 (Ω = 8°/s); the UKF's Ω bias is practically absent (≤0.35 deg./s vs. ≈1 deg/s RMSE), unlike the EKF's order-of-magnitude larger, sign-changing bias (–2.8 to +1.1 deg./s).

Table 2. Unscented Kalman filter vs. extended Kalman filter at Ω = 6°/s (nominal maneuver), N_{run} = 545

Radar	ΔΩ, deg./s		Gain in Ω, ×	Δpos, m		Gain in pos., ×	Δ*v*, m/s		Gain in *v*, ×
	UKF	EKF		UKF	EKF		UKF	EKF	
R1	0.82	3.68	4.5	349	396	1.1	35.0	87.2	2.5
R2	1.04	6.31	6.1	292	362	1.2	28.5	140.3	4.9
R3	0.93	9.35	10.0	428	691	1.6	24.9	273.1	11.0
R4	0.88	2.02	2.3	369	380	1.0	37.7	54.5	1.4
R5	0.92	3.92	4.3	265	306	1.2	11.4	36.5	3.2
R6	0.85	4.46	5.3	155	252	1.6	8.0	26.7	3.3
R7	0.99	4.23	4.3	331	348	1.1	18.1	56.3	3.5
R8	0.90	2.29	2.5	543	570	1.1	40.6	65.3	1.6

Spread of the estimates and convergence dynamics. Tab. 2 reports only the pooled RMSE over the entire maneuver; its spread across Monte-Carlo realizations and its convergence dynamics vs. scan index *k* are shown next, again for the nominal maneuver Ω = 6°/s.

Fig. 1 shows the UKF's advantage lies not only in average accuracy but in stability: the EKF's interquartile range for Ω is noticeably wider and asymmetric for most radars, meaning it regularly produces realizations with anomalously large error, whereas the UKF produces virtually none.

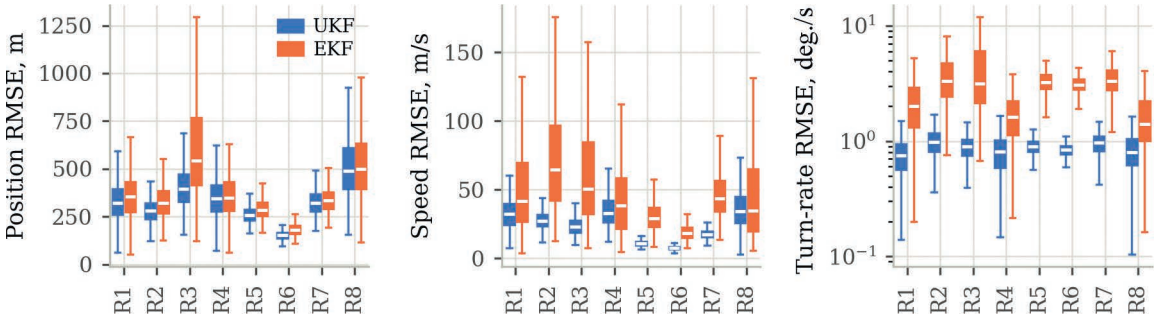


Fig. 1. Spread of the position, speed, and turn-rate root-mean-square error over N_{run} = 545 Monte-Carlo realizations: UKF – blue; EKF – orange; box – interquartile range (IQR); whisker – 1.5 IQR

The dynamics vs. scan index (Fig. 2, 3) reveal the mechanism behind Tab. 2 pooled RMSE. Both algorithms coincide at the first scan (same initialization); the UKF then reaches ≈1°/s within one–two scans and holds it, whereas the EKF diverges systematically as the accumulated turn angle $\Omega_k T$ grows the linearization error of $\mathbf{B}_k$ – monotonically for most radars, but oscillating for R5, R6 (short T = 1–2 s),

where repeated reinitialization on near-straight segments is followed by renewed growth. The divergence is universal, ruling out initial conditions as the cause; it is weakest for R4, R8 (gains 2.3 and 2.5×), whose long scan period (T = 10 s) gives the EKF too few scans to accumulate its usual error.

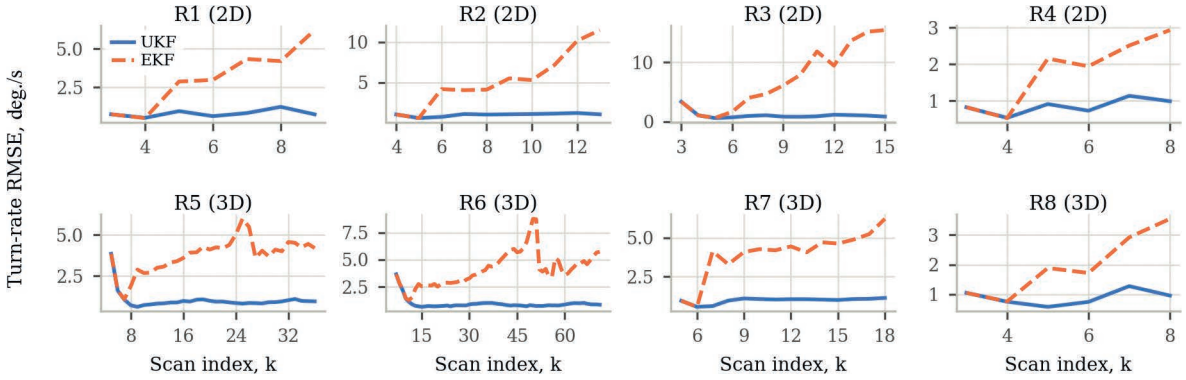


Fig. 2. Turn-rate root-mean-square error (averaged over N_{run} = 545 realizations)

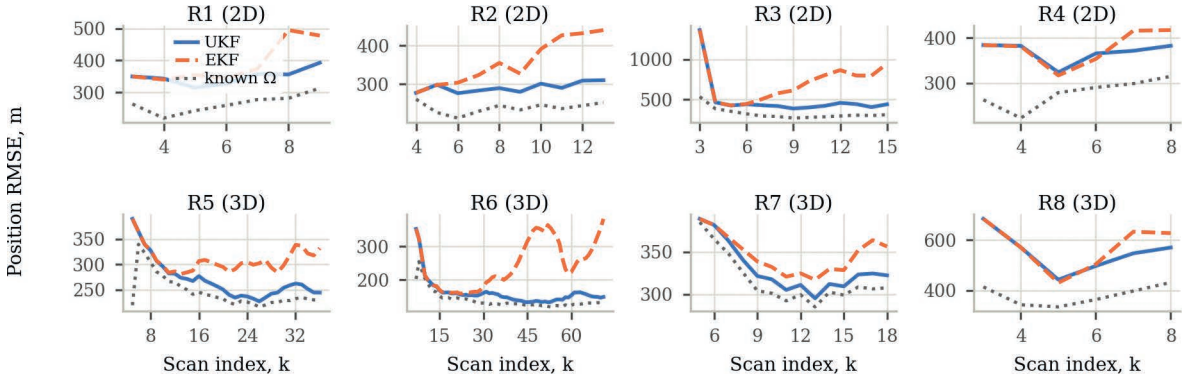


Fig. 3. Position root-mean-square error (dotted – the potentially achievable error with Ω known)

Comparison against the potentially achievable error (dotted curve in Fig. 3) shows that, once the transient passes, the UKF's position RMSE stays close to the noise-only bound, while the EKF's departs systematically; the same pattern holds for speed (Tab. 2). Unscented filtering of the turn rate thus improves not only Ω itself, but also brings position and velocity accuracy close to the achievable level.

Conclusion

1. Once Ω is included in the augmented state vector, the state-transition matrix becomes a nonlinear function of Ω, so linearizing the motion model introduces an error beyond the previously studied [18] measurement-model linearization error.

2. A discrete filter for jointly estimating a target's coordinates, velocity, and turn rate Ω, based on the unscented transform and requiring no Jacobian computation for either model, is proposed.

3. A weighted-least-squares initialization method is proposed, supplying initial state-vector estimates (Ω included) with their covariance, without a priori target knowledge; solved as a separable least-squares problem linear in the remaining components for fixed Ω (no initial guess needed), with the number of plots chosen adaptively and the search over Ω confined to $|\Omega| < 180°/T$.

4. A Monte-Carlo study for eight radars and five Ω values (40 combinations, N_{run} = 545 each) shows the Unscented Kalman filter Ω root-mean-square error averaging 4,3× smaller (median 4.0; range 1.4–14.0) than the linearized extended Kalman filter, versus a more modest 1.2× gain in position root-mean-square error – consistent with the mechanism above: coordinates are observed directly (nonzero H_k), Ω only through the cross-covariance generated by $\mathbf{B}_k$.

5. Directions for further research: algorithm behavior under a time-varying turn rate, and an adaptive bank of unscented filters tuned to different Ω values (by analogy with IMM banks [5], but for maneuver-intensity rather than motion-model hypotheses) – a separate publication.

6. This work was supported by a grant from the Belarusian Republican Foundation for Fundamental Research (Project No T26UZB-007) and the Ministry of Higher Education, Science and Innovation of the Republic of Uzbekistan (Project No FL-10425067114).

References

1. Shirman Ya. D. (2007) *Radioelectronic Systems. Foundations and Theory*. Moscow, Radiotekhnika Publ. (in Russian).
2. Artemyev V. M., Khmarskiy P. A., Naumov A. O. (2025) Reducing Radar Measurement Errors Using Ionosphere and Magnetosphere Monitoring Data. *Doklady BGUIR*. 23 (4), 54–62. https://doi.org/10.35596/1729-7648-2025-23-4-54-62 (in Russian).
3. Bar-Shalom Y., Li X. R. (2011) *Trajectory Processing. Principles, Methods and Algorithms*. Moscow (in Russian).
4. Li X. R., Jilkov V. P. (2003) Survey of Maneuvering Target Tracking: Part I – Dynamic Models. *IEEE Trans. Aerospace and Electronic Systems*. 39 (4), 1333–1364. https://doi.org/10.1109/TAES.2003.1261132.
5. Solonar A. S., Khmarskiy P. A., Mikhalkovski A. A. (2013) Features of Filtering Using Coordinated Turn Models. *Doklady BGUIR*. (4), 67–73 (in Russian).
6. Rong D., Wang Y. (2024) An Adaptive Spatial Target Tracking Method Based on Unscented Kalman Filter. *Sensors*. 24 (18), 6094. https://doi.org/10.3390/s24186094.
7. Dong Y., Li W., Li D., Liu C., Xue W. (2024) Intelligent Tracking Method for Aerial Maneuvering Target Based on Unscented Kalman Filter. *Remote Sensing*. 16 (17). https://doi.org/10.3390/rs16173301.
8. Ye X., Wang J., Wu D., Zhang Y., Li B. (2023) A Novel Adaptive Robust Cubature Kalman Filter for Maneuvering Target Tracking with Model Uncertainty and Abnormal Measurement Noises. *Sensors*. 23 (15). https://doi.org/10.3390/s23156966.
9. Mallick M., Tian X., Zhu Y., Morelande M. (2022) Angle-Only Filtering of a Maneuvering Target in 3D. *Sensors*. 22 (4). https://doi.org/10.3390/s22041422.
10. Coelho M. de F., Bousson K., Ahmed K. (2021) An Improved Extended Kalman Filter for Radar Tracking of Satellite Trajectories. *Designs*. 5 (3). https://doi.org/10.3390/designs5030054.
11. Chen Y. W., Tu K. M. (2022) Robust Self-Adaptive Kalman Filter with Application in Target Tracking. *Measurement and Control*. 55 (9–10), 935–944. https://doi.org/10.1177/00202940221083548.
12. Tian F., Guo X., Fu W. (2024) Target Tracking Algorithm Based on Adaptive Strong Tracking Extended Kalman Filter. *Electronics*. 13 (3). https://doi.org/10.3390/electronics13030652.
13. Edrisi S., Enayati J., Rahimnejad A., Gadsden S. A. (2024) A Monte Carlo-Based Iterative Extended Kalman Filter for Bearings-Only Tracking of Sea Targets. *Sensors*. 24 (7). https://doi.org/10.3390/s24072087.
14. Zhang W., Zhao X., Liu Z., Liu K., Chen B. (2023) Converted State Equation Kalman Filter for Nonlinear Maneuvering Target Tracking. *Signal Processing*. 202. https://doi.org/10.1016/j.sigpro.2022.108741.
15. Cheng T., Cao C. (2023) Kalman Filter Based on Intermediate Transition State for Radar Target Tracking with Nonlinear Measurements. *Digital Signal Processing*. 143. https://doi.org/10.1016/j.dsp.2023.104251.
16. Li X., Lu B., Li Y., Lu X., Jin H. (2023) Adaptive Interacting Multiple Model for Underwater Maneuvering Target Tracking with One-Step Randomly Delayed Measurements. *Ocean Engineering*. 280. https://doi.org/10.1016/j.oceaneng.2023.114933.
17. Hu P., Zhang M., Zhang R., Wu Q., Yang A. (2021) Correlation Method and Kalman Filter-Based Adaptive Angle Rate Estimation for Time-Varying Periodic Signals of the Attitude and Heading Reference System. *Mechanical Systems and Signal Processing*. 156. https://doi.org/10.1016/j.ymssp.2021.107695.
18. Solonar A. S., Khmarskiy P. A. (2014) The Conditions of Observation Research for Extended Kalman Filter Goodness-of-Fit Using Monte-Carlo Method. *Doklady BGUIR*. (7), 71–77 (in Russian).
19. Khmarskiy P. A., Solonar A. S. (2012) Choice Effect of Input Action Models on Measuring Accuracy for Extended Kalman Filters. *Doklady BGUIR*. (7), 47–53 (in Russian).
20. Khmarskiy P. A., Solonar A. S. (2012) Features of Adaptive Extended Kalman Filter Implementations. *Doklady BGUIR*. (8), 57–63 (in Russian).
21. Julier S. J., Uhlmann J. K. (2004) Unscented Filtering and Nonlinear Estimation. *Proceedings of the IEEE*. 92 (3), 401–422. https://doi.org/10.1109/JPROC.2003.823141.
22. Khmarskiy P. A., Solonar A. S. (2013) Features of Unscented Kalman Filter Performance Using Polar Measurements. *Doklady BGUIR*. (2), 79–85 (in Russian).

Received: 28 August 2026 Accepted: 14 September 2026

Authors' contribution

Khmarski P. developed the unscented filtering algorithm for the augmented state vector, performed the modeling, summarized and interpreted the results, and prepared the manuscript.

Artemiev V. substantiated the research concept and formulated the idea, goals and objectives.

Naumov A. collected and systematized the data, edited the manuscript, and prepared graphic materials.

Bondarenko A. obtained the analytical form of the state-transition matrix and established the unobservability of the turn rate in the measurement Jacobian, proposed the method for setting the filter's initial values by weighted least squares (initialization) and substantiated its covariance.

Muxammedov B. prepared the sets of radar characteristics and observation conditions for the modeling and took part in verifying the results.

Information about the authors

Khmarski P., Cand. Sci. (Tech.), Associate Professor, Leading Researcher, Institute of Applied Physics of the National Academy of Sciences of Belarus (IAP NAS Belarus)

Artemiev V., Corr. Member of the National Academy of Sciences of Belarus**,** Dr. Sci. (Tech.), Professor, Principal Researcher, IAP NAS Belarus

Naumov A., Cand. Sci. (Phys. and Math.), Head of Laboratory, IAP NAS Belarus

Bondarenko A., Lecturer, Military Academy of the Republic of Belarus

Muxammedov B., Head of the Research Laboratory, Institute of Military Aviation of the University of Military Security and Defense of the Republic of Uzbekistan

Address for correspondence

220072, Republic of Belarus,
Minsk, Akademicheskaya St., 16
Institute of Applied Physics
of the National Academy of Sciences of Belarus
Tel.: +375 17 300-73-98
E-mail: pierre2009@mail.ru
Khmarski Petr